The Astrophysical Journal, 643:797–803, 2006 June 1

DENSITY PROFILES OF COLLISIONLESS EQUILIBRIA. I. SPHERICAL ISOTROPIC SYSTEMS

Eric I. Barnes and Liliya L. R. Williams
Department of Astronomy, University of Minnesota, Minneapolis, MN 55455; barnes@astro.umn.edu, llrw@astro.umn.edu

Arif Babul[1]
Department of Physics and Astronomy, University of Victoria, BC, Canada; babul@uvic.ca

and

Julianne J. Dalcanton[2]
Department of Astronomy, University of Washington, Box 351580, Seattle, WA 98195; jd@astro.washington.edu
Received 2005 October 11; accepted 2006 January 31

ABSTRACT

We investigate the connection between collisionless equilibria and the phase-space relation between density ρ and velocity dispersion σ found in simulations of dark matter halo formation, $F = \rho/\sigma^3 \propto r^{-\alpha}$. Understanding this relation will shed light on the physics relevant to collisionless collapse and on the subsequent structures formed. We show that empirical density profiles that provide good fits to N-body halos also happen to have nearly scale-free ρ/σ^3 distributions when in equilibrium. We have also done a preliminary investigation of variables other than r that may match or supersede the correlation with F. In the same vein, we show that ρ/σ^m, where $m = 3$, is the most appropriate combination to use in discussions of the power-law relationship. Since the mechanical equilibrium condition that characterizes the final systems does not by itself lead to power-law F distributions, our findings prompt us to posit that dynamical collapse processes (such as violent relaxation) are responsible for the radial power-law nature of the ρ/σ^3 distributions of virialized systems.

Subject headings: dark matter — galaxies: kinematics and dynamics — galaxies: structure

1. INTRODUCTION

The "poor man's" phase-space density proxy $F = \rho/\sigma^3$, where ρ is density and σ is total velocity dispersion, is a power law in radius ($F \propto r^{-\alpha}$) for a surprising variety of self-gravitating, collisionless equilibria. Isothermal systems have $\rho \propto r^{-2}$ and constant σ, giving $\alpha = 2$. A broader class of systems with power-law behavior in both ρ and σ also naturally produce power-law behavior for F. For example, the self-similar collisionless infall models in Bertschinger (1985, § 4) have $\rho \propto r^{-9/4}$ and $\sigma \propto r^{-1/8}$, leading to $\alpha = 1.875$. More surprising is that systems in which neither ρ nor σ are power laws can still possess F distributions that are. For example, there is a growing body of evidence, supported by results from simulations of increasingly higher resolution and detail, that seems to suggest that collisionless halos formed in cosmological simulations are characterized by nearly scale-free F distributions, although they have decidedly non–power-law density profiles. This was first noted by Taylor & Navarro (2001), who at the time determined that $\alpha = 1.875$ over 3 orders of magnitude in radius. This value of α, coincidently, is the same as that derived by Bertschinger (1985). More recent N-body simulations have produced α-values of 1.95 (Raisa et al. 2004), 1.90 (Ascasibar et al. 2004), and 1.84 (Dehnen & McLaughlin [2005], based on the simulations in Diemand et al. [2004a, 2004b]). Austin et al. (2005) report that a very different, semianalytical halo formation method results in power-law F distributions over similar radial ranges. However, these authors find a range of α-values (including 1.875) that depend on initial conditions. As this formation method is much simpler than an N-body evolution but still reproduces scale-free F, the physics responsible for the distribution must be common to both techniques. One such process is violent relaxation. In this work, we use "violent relaxation" as shorthand for the incomplete relaxation process that is due to the varying of potential during collapse rather than the strict, complete relaxation discussed in Lynden-Bell (1967). Also, in the Austin et al. (2005) work, it is shown that in a totally isotropic system the Jeans equation can be solved analytically and that there is a "special" $\alpha = 35/18 = 1.94\bar{4}$.

It appears that power-law distributions of F are robust features of collisionless equilibria. The exponents of the power laws vary, but cluster near values $\lesssim 2$. This paper is part of a continuing series of investigations aimed at understanding the ubiquity and the origin of the phenomenon. We specifically want to exploit its occurrence to gain insights into the processes governing the virialization of collisionless halos.

In this paper we review the conditions for hydrostatic equilibrium, the Jeans equation. By examining density profiles motivated by N-body simulations and analyzing the associated F distributions, in § 3 we demonstrate that the Jeans equation by itself is not sufficient to force a power law for ρ/σ^3. At present, we restrict ourselves to spherical equilibria with isotropic velocity distributions. Interestingly, typical density profiles that are used to characterize data from cosmological N-body simulations all seem to have nearly scale-free F distributions, as do halos that are formed semianalytically (Austin et al. 2005). This aspect of N-body and semianalytically generated halos is certainly unexpected, and consequently, in § 4 we investigate the implications of explicitly imposing the requirement of scale-free ρ/σ^3 on the density profiles of equilibrium structures. We summarize our findings in the final section.

2. EMPIRICAL DENSITY PROFILES

In this work we focus on several specific density profiles, shown in Figures 1 and 2. The standard Navarro-Frenk-White

[1] Leverhulme Visiting Professor, Universities of Oxford and Durham.
[2] Alfred P. Sloan Foundation Fellow.

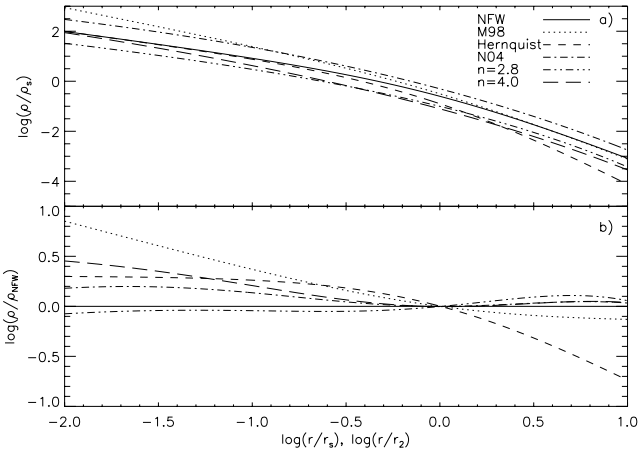

FIG. 1.—Plots showing the NFW (*solid line*), Moore et al. (1998; *dotted line*), Hernquist (1990; *dashed line*), Navarro et al. (2004; *dash-dotted line*), Sérsic $n = 2.8$ (*double-dot–dashed line*), and Sérsic $n = 4.0$ (*long-dashed line*) density distributions. The line types have the same meaning in both plots. (*a*) The log-log density profiles. The vertical normalization is arbitrary and the curves have been somewhat separated to aid identification. (*b*) The log-log density profiles of the same distributions divided the NFW (*horizontal solid line*). These ratio profiles have been normalized to agree at the scale radius.

(Navarro et al. 1996, 1997, hereafter NFW), Moore et al. (1998, hereafter M98), and Hernquist (1990) (*solid, dotted, and dashed lines, respectively*) profiles are examples of dual–power-law distributions with differing asymptotic behaviors that have been used to fit density profiles of cosmological *N*-body halos. The generalized dual–power-law profile has the form

$$\frac{\rho}{\rho_s} = \left(\frac{r}{r_s}\right)^{-c_1}\left(1+\frac{r}{r_s}\right)^{-c_2}, \tag{1}$$

where ρ_s and r_s are a scale density and length, respectively. The exponents c_1 and c_2 determine the asymptotic power-law behavior of the profile: NFW ($c_1 = 1$, $c_2 = 2$); M98 ($c_1 = 1.5 = c_2$); and Hernquist ($c_1 = 1$, $c_2 = 3$). We define the negative logarithmic density slope to be $\gamma \equiv -d\log(\rho/\rho_s)/d\log(r/r_s)$. For generalized dual–power-law profiles, the γ distributions are given by

$$\gamma = \frac{c_1 + (c_1 + c_2)(r/r_s)}{1 + (r/r_s)}. \tag{2}$$

The Navarro et al. (2004) profile (*dash-dotted line*) has been proposed as an improvement over NFW for describing high-resolution cosmological *N*-body density profiles. This profile never displays power-law behavior; instead, the logarithmic density slope changes continuously with *r*. The expression that generates this curve is

$$\ln\left(\frac{\rho}{\rho_2}\right) = -\left(\frac{2}{\mu}\right)\left[\left(\frac{r}{r_2}\right)^{\mu} - 1\right], \tag{3}$$

where r_2 is the radius at which $\gamma = 2$ and ρ_2 is the density at that radius. The corresponding γ profile is

$$\gamma = 2\left(\frac{r}{r_2}\right)^{\mu}. \tag{4}$$

As Navarro et al. (2004) found that $\mu = 0.17$ best fit several *N*-body halo profiles, we refer to profiles (ρ and γ) with $\mu = 0.17$ as N04 profiles, but we consider $0.001 \leq \mu \leq 0.22$.

The final profile type that we consider is the Sérsic function (Sérsic 1968). The Sérsic function is expressed analytically as

$$\ln\left(\frac{\Sigma}{\Sigma_s}\right) = -a_n\left[\left(\frac{R}{R_s}\right)^{1/n} - 1\right], \tag{5}$$

where Σ is surface density, R is projected distance, n determines the shape of the profile, and a_n is an n-dependent constant chosen so that the projected mass interior to R_s is equal to the projected mass interior to $R = r_2$ for the N04 profile (eq. [3]). This differs from the usual definition of the Sérsic constant, which demands the projected mass within R_s be half the total mass. Unfortunately, Sérsic profiles do not readily provide analytical expressions for ρ or γ (but see Trujillo et al. 2002 and Graham et al. 2005). The double-dot–dashed and long-dashed lines in Figure 1 show the calculated deprojected density distributions for $n = 2.9$ and $n = 4.0$ (de Vaucouleurs profile), respectively. Larger (smaller) n-values reduce (increase) the difference between the inner and outer logarithmic density slopes. Dalcanton & Hogan (2001) and Merritt et al. (2005) both suggest that the Sérsic profile describes the results of *N*-body simulations at least as well as the previously discussed forms. Further, Dalcanton & Hogan (2001) point out that $n \lesssim 4$ Sérsic and NFW profiles have similar behaviors, while Merritt et al. (2005) find that $n \approx 3$ provides the best fit to their dwarf- and galaxy-sized halos.

3. ρ/σ^3 DISTRIBUTIONS AND EQUILIBRIUM

Mechanical equilibrium for a spherical and isotropic collisionless system is determined through the Jeans equation (Jeans 1919; Binney & Tremaine 1987),

$$\frac{d}{dr}\left[\rho(r)\sigma^2(r)\right] = -3G\rho(r)\frac{M(r)}{r^2}, \tag{6}$$

where $M(r)$ is the mass enclosed at radius r and the factor of 3 comes from the definition $\sigma^2 = \sigma_r^2 + \sigma_\theta^2 + \sigma_\phi^2$ and the isotropy of the system. This equation certainly links ρ and σ, but does it alone impose power-law F distributions?

3.1. *Specific Distributions*

We demonstrate that the answer is no by providing a counterexample. Inserting the Hernquist density profile into equation (6), we solve for σ and thereby ensure that the halo is in equilibrium. The resulting F distribution is shown as a solid line in Figures 2*a* and 2*b*. In the top panels of this figure, the dashed lines have slopes of -1.875, the dotted lines have slopes of $-35/18$, and each line is normalized to the F value at $\log(r/r_s) = 0$. The curves in the bottom panels highlight departures from the best-fit power-law behavior (*horizontal double-dot–dashed lines*). The dashed and dotted lines denote the same power laws as in the top panels, but scaled to the best-fit slope. We use $\alpha = 1.875$ as a fiducial value because it is the result of straightforward analytical calculation (Bertschinger 1985), as well as being representative of the mean of the *N*-body results discussed in § 1. At the same time, we also highlight the analytically motivated $\alpha = 35/18$ (Austin et al. 2005). The abscissa range for the figure reflects that halos are usually resolved over roughly 3 orders of magnitude, from the virial radius [$\log(r/r_s) \approx 1$] to about 1/1000 of the virial radius [$\log(r/r_s) \approx -2$]. The double-dot–dashed lines in the bottom panels indicate the best linear fits to the F profiles. The dotted and dashed lines represent the same lines as in the top panel rescaled to the best linear fit slope. The α-values indicate the slope (modulo a minus sign) that the best linear fit would have in the top panel.

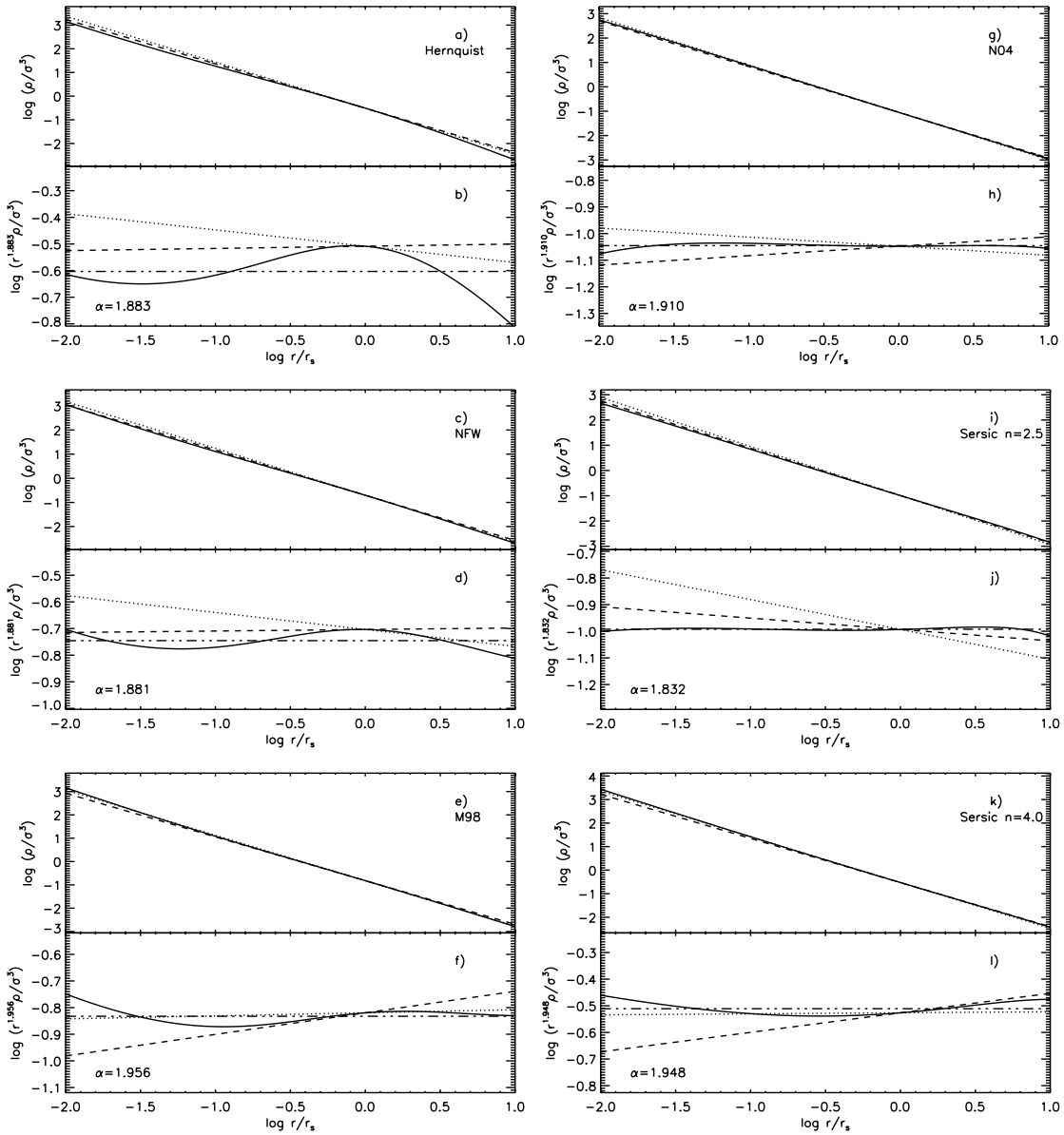

FIG. 2.—Plots showing the raw F distributions (a, c, e, g, i, k) and versions scaled to highlight departures from a pure power law (b, d, f, h, j, l). The dashed and dotted lines show the behavior of power-law F distributions with $\alpha = 1.875$ and $\alpha = 35/18$, respectively. The α-values indicated in the bottom panels are the slopes of the lines that best-fit the scaled profiles. Also in the bottom panels, the scaled best linear fits are the double-dot–dashed horizontal lines, and the dotted and dashed lines are the scaled power laws corresponding to the lines in the top panels. The density profiles are noted in the plots: (a, b) Hernquist (1990); (c, d) NFW; (e, f) Moore et al. (1998); (g, h) Navarro et al. (2004); (i, j) Sérsic $n = 2.5$; and (k, l) Sérsic $n = 4.0$.

We use the rms deviations $\Delta_{\rm rms}$ between the F distributions and the best power-law fits to quantify how close to a power law each F is. These deviations are calculated over the resolved range of N-body halos, from $\log(r/r_s) \approx -2$ to $\log(r/r_s) \approx 1$. We adopt the following convention for the rest of the paper: F distributions with $\Delta_{\rm rms} \leq 0.05$ will be considered power laws, those with $\Delta_{\rm rms} > 0.05$ will not. This approximately reflects the level at which one can detect a power law by eye, e.g., by looking at Figure 2a. With this criterion, the Hernquist profile, with $\Delta_{\rm rms} = 0.07$, is evidence that simple mechanical equilibrium does not enforce power-law F behavior. The Hernquist profile is not unique in this regard; King models (King 1966, not discussed in detail here) also produce F distributions that have quite obvious deviations from power-law shapes.

Having found these counterexamples, we now demonstrate that the other empirical density profiles from § 2 generally lead to scale-free F distributions. In Figure 2 we present the F distributions calculated by solving equation (6) using the NFW (Figs. 2c and 2d), M98 (Figs. 2e and 2f), and N04 (Figs. 2g and 2h) density profiles. These profiles have power-law F distributions with $\Delta_{\rm rms} \lesssim 0.03$ and $\alpha = 1.881$, 1.956, and 1.910 for NFW, M98, and N04, respectively. The N04 profile produces the best power-law F distribution of these three models, with $\Delta_{\rm rms} = 0.007$. The NFW and M98 profiles are poorer (but still acceptable) power laws with $\Delta_{\rm rms} \approx 0.03$. Sérsic profiles also produce power-law F distributions, with the best power-law F ($n = 2.5$, $\Delta_{\rm rms} = 0.005$, $\alpha = 1.832$) shown in Figures 2i and 2j. We also include the results from the de Vaucouleurs profile (Sérsic $n = 4.0$) Figures 2k and 2l. This range of α-values (1.83–1.96) is approximately the same as the range of results from N-body simulations (see § 1). These findings are also in broad agreement with the results of Graham et al. (2005).

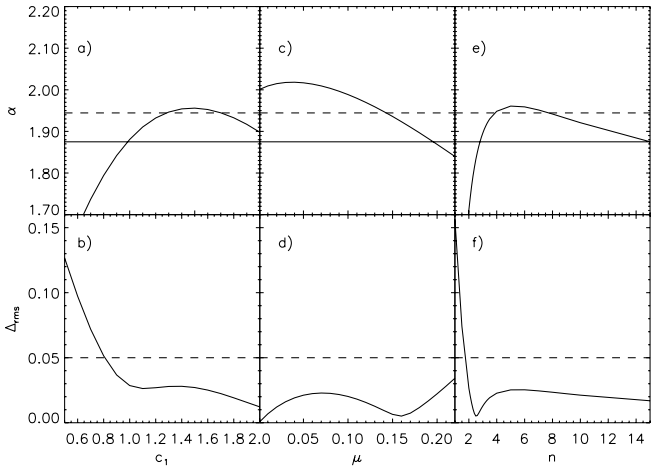

FIG. 3.—Plot of the α and $\Delta_{\rm rms}$ values vs. the shape parameters for (a, b) generalized dual–power-law profiles, (c, d) N04 profiles, and (e,f) Sérsic profiles. The shape parameters are c_1 ($c_2 = 3 - c_1$), μ, and n for the dual–power-law, N04, and Sérsic profiles, respectively. In the top panels, the solid line lies at $\alpha = 1.875$ and the dashed line marks $\alpha = 35/18$. The dashed line in the bottom panels illustrates the acceptable power-law cutoff value of $\Delta_{\rm rms} = 0.05$.

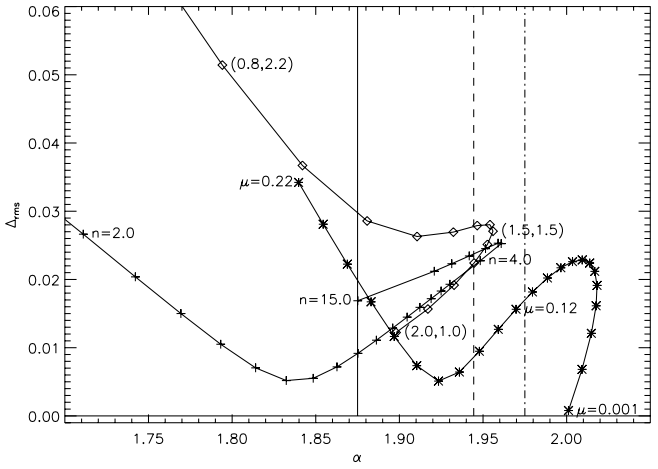

FIG. 4.—Plot shows α vs. $\Delta_{\rm rms}$ for generalized dual–power-law (*diamonds*), N04 (*asterisks*), and Sérsic (*plus signs*) profiles. Along the Sérsic track, the n values increase from 2 to 15, with a turnaround point at $n = 5$. The μ values decrease from left to right (0.22 → 0.001) along the N04 track. The top leftmost diamond has ($c_1 = 0.8, c_2 = 2.2$), the diamond with the largest α corresponds to the M98 profile ($c_1 = c_2 = 1.5$), and the diamond with the smallest $\Delta_{\rm rms}$ has ($c_1 = 2.0, c_2 = 1.0$). The NFW ($c_1 = 1.0, c_2 = 2.0$) profile is marked by the diamond nearest to the solid line at $\alpha = 1.875$. The dashed and dash-dotted lines mark $\alpha = 35/18$ and $\alpha = 1.975$, respectively.

3.2. *General Distributions*

In addition to these specific profiles, we have also examined the generic forms of equations (1), (3), and (5). Varying the shape parameters (c_1, c_2, μ, n) of these profiles allows us to (1) find the profiles that have the best power-law F behavior and (2) determine the ranges of α-values that each profile supports. We summarize the findings in Figures 3 and 4.

Three classes of profiles are presented separately in Figure 3 to show the impact of the shape parameters on the F distributions. Figures 3*a* and 3*b* display the results for generalized dual–power-law profiles with the constraint that $c_1 + c_2 = 3$ (like NFW and M98) and $0.5 \le c_1 \le 2.0$. One can see that $\alpha = 1.875$ is obtained when $c_1 \approx 1.0$ ($c_2 \approx 2.0$), very nearly the canonical NFW profile. However, the shallow local minimum in Figure 3*b* around $c_1 = 1.1$ indicates that the NFW profile does not give the best power-law F (for isotropic systems).[3] The shallowness of this minimum suggests that all values $1.0 \lesssim c_1 \lesssim 1.5$ give similar quality power-law ρ/σ^3 distributions. We note that the M98 profile ($c_1 = 1.5$) produces an α-value closer to the analytical value of 35/18, with the ($c_1 = 1.3$) case providing the best fit to $\alpha = 35/18$. We have also investigated a few profiles with $c_1 + c_2 = 4$ and found that they do not form acceptable power-law F distributions. Like the Hernquist profile ($c_1 = 1$, $c_2 = 3$), the $\Delta_{\rm rms}$ values for these profiles are always >0.05. The Navarro et al. (2004) profiles with $0.001 \le \mu \le 0.22$ give rise to Figures 3*c* and 3*d*. The F distribution that produces the best power law has $\mu \approx 0.16$, which is very close to the best-fit value $\mu = 0.17$ from Navarro et al. (2004). For $\mu \approx 0.14$, the corresponding $\alpha \approx 35/18$. This range in μ values is consistent with halos found in the simulations of Navarro et al. (2004), $0.1 \lesssim \mu \lesssim 0.2$. Among Sérsic profiles with $2.0 \le n \le 15.0$ (Figs. 3*e* and 3*f*), the model at which $\Delta_{\rm rms}$ is minimum has $n = 2.5$. This n value lies in the range of values found in the Merritt et al. (2005) study. Interestingly, the Sérsic profile that produces $\alpha = 35/18$ has $n \lesssim 4$, basically a de Vaucouleurs profile.

Pursuing this further, we turn to Figure 4, which combines the results from the three profile types by relating α and $\Delta_{\rm rms}$ values. The plus signs represent Sérsic profile values, asterisks mark the Navarro et al. 2004 values, and diamonds show generalized dual–power-law values. The vertical structure of this plot illustrates that the Navarro et al. (2004) and Sérsic profiles generally result in better power-law F distributions than the dual–power-law form. Interestingly, if we think of the various simulation-inspired profiles in chronological order (NFW, M98, and N04), it appears that the ρ/σ^3 distributions are becoming better power laws as the number of particles in simulations increases and the simulations themselves improve. Such a trend may be due to a decreased impact by two-body relaxation (which masks the dynamics relevant to actual halos and decreases in importance with increasing particle numbers), or it may be that the larger particle numbers allow simulations to more faithfully reflect the pertinent physics, e.g., violent relaxation.

In the horizontal direction of Figure 4, we clearly see that the profile types produce their best power law at varying α-values. However, the minimum value of $\Delta_{\rm rms}$ for all the profiles occur in a relatively narrow range of α-values, between 1.84 and 1.97, close to the analytically derived value of $\alpha = 1.94\bar{4}$. One thing to keep in mind is that this study deals only with isotropic systems. It could be that simulated N-body halos, which have anisotropic velocity distributions (Hansen & Moore 2006; Barnes et al. 2005), are sufficiently different from these isotropic models to cause the offsets.

3.3. *A More Fundamental Relation?*

The scale-free relationship between F and r has been firmly established, but we would like to know if there is a more dynamically relevant quantity that shows a similar power-law correlation with F. The list of candidate quantities is long, but we focus on two choices: enclosed mass $M(r)$ and a proxy for the radial action $r\sigma_r$. The $\log F$ versus $\log M$ plots do not have power-law forms for any of the distributions. On the other hand, the $\log F$ versus $\log r\sigma_r$ curves do have approximately scale-free shapes,

[3] We point out that all of these profile types can produce perfect power-law F distributions ($\Delta_{\rm rms} = 0$) in the limit that the density becomes a pure power law: $c_1 \to 3$, $c_2 \to 0$ for the generalized dual–power-law form, $\mu \to 0$ for the Navarro et al. (2004) form, and $n \to \infty$ for the Sérsic form. Since these pure power-law density profiles result in unphysical infinite mass objects, we define the "best" power-law F distributions to be determined by the local minima apparent in the bottom panels of Fig. 3.

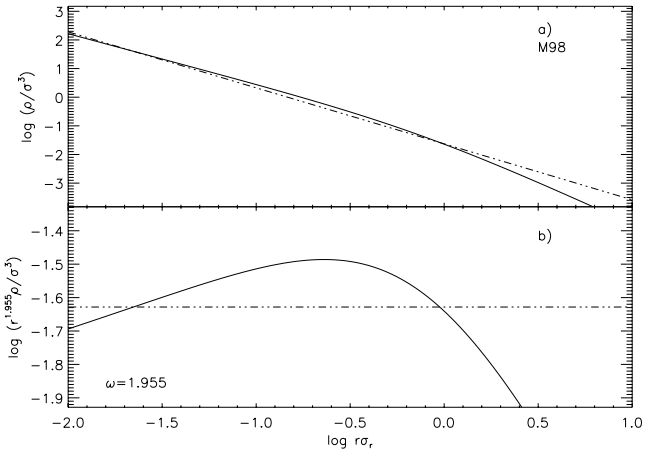

FIG. 5.—Representative curves showing the relationship between ρ/σ^3 and the radial action proxy $r\sigma_r$. These specific curves are for the M98 profile and should be compared to those in Figs. 2*e* and 2*f*. Panel *a* shows the raw correlation between $\log F$ and $\log r\sigma_r$ along with the best linear fit (*double-dot–dashed line*). Panel *b* displays the residuals between the best-linear fit and the actual correlation. The slope of the best-fit line is given by the ω value.

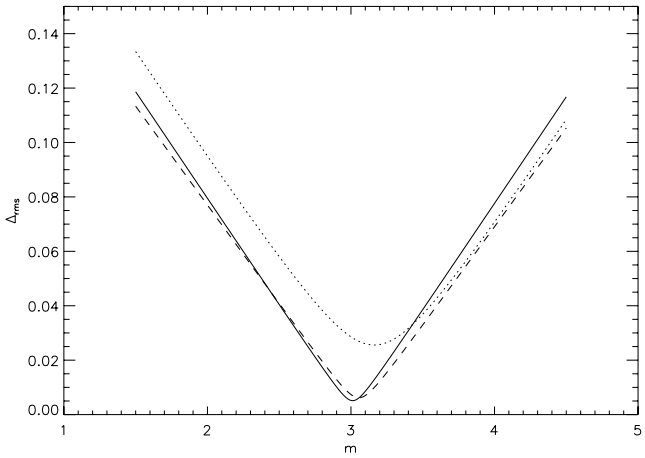

FIG. 6.—Curves showing that the best ρ/σ^m vs. r power law occurs when $m = 3$. The dotted line is the result of varying m for an NFW profile, while the dashed and solid lines illustrate the variations for N04 and Sérsic $n = 2.5$ profiles, respectively.

as shown in Figure 5*a*. The best-fit line to this curve has a slope ($\omega = 1.955$) that is very close the slope in Figure 2*e* ($\alpha = 1.956$). However, the comparison between the residuals shown in Figure 5*b* and those in Figure 2*f* demonstrate that F versus r is the better scale-free relation. Indeed, the near power-law relation between F and $r\sigma_r$ occurs because σ_r has a very weak relation on r, making F versus $r\sigma_r$ very similar to F versus r.

Hoeft et al. (2004) find that a nontrivial function of potential accurately describes the velocity dispersion profile in *N*-body halos. Utilizing a more general form of this function of potential,

$$A = \Phi^a(\Phi_{\rm out} - \Phi)^b, \tag{7}$$

we have investigated whether or not F versus A provides a superior power-law relation to F versus r. We find that with appropriate choices of a, b, and $\Phi_{\rm out}$, a power law can be found for F versus A that is of comparable quality to that for F versus r. However, we find that the degrees of freedom present in this function allow it to closely resemble r itself, making this function unenlightening. Despite the results of this brief search for a more physically fundamental relation, we plan to continue investigating alternative dynamical quantities.

One could also question whether or not our F function is the most illuminating choice of combination of ρ and σ. Certainly, ρ/σ^3 is an interesting quantity, as it has the dimensions of phase-space density, but would ρ/σ^m work just as well (R. Henriksen 2006, private communication)? For the NFW, N04, and Sérsic functions, the answer is no. The deviations from a power-law distribution rapidly increase as m varies from 3 (over the interesting radial range $-2 \le \log r/r_s \le 1$). This affinity for $m = 3$ is obvious in Figure 6, which shows the amplitude of the residuals from a power-law F versus r relationship as m is varied from 1.5 to 4.5.

In this section we have shown that the condition of hydrostatic equilibrium by itself does not produce power-law ρ/σ^3. However, the density profiles that are used to fit the data from cosmological *N*-body simulations all seem to have nearly scale-free ρ/σ^3 distributions, unlike the Hernquist and King profiles. We have also tried, in vain, to find more physically meaningful correlations between F and other quantities; enclosed mass, $r\sigma_r$, etc. Furthermore, halos formed semianalytically, through violent relaxation (Lynden-Bell 1967), also display $F \propto r^{-\alpha}$ (Austin et al. 2005). This aspect of *N*-body and semianalytically generated halos is certainly unexpected and prompts us to consider systems that have explicitly scale-free ρ/σ^3.

4. THE CONSTRAINED JEANS EQUATION

Imposing the constraint that $\rho/\sigma^3 = (\rho_0/v_0^3)(r/r_0)^{-\alpha}$ and using the dimensionless variables $x \equiv r/r_0$ and $y \equiv \rho/\rho_0$, we rewrite equation (6) as

$$-\frac{x^2}{y}\left[\frac{d}{dx}\left(y^{5/3}x^{2\alpha/3}\right)\right] = BM(x), \tag{8}$$

where $B = 3G/r_0v_0^2$. Differentiating this equation with respect to x gives us

$$\frac{d}{dx}\left\{-\frac{x^2}{y}\left[\frac{d}{dx}\left(y^{5/3}x^{2\alpha/3}\right)\right]\right\} = Cyx^2, \tag{9}$$

where $C = 12\pi\rho_0 r_0^2/v_0^2$. This expression is equivalent to that presented in Taylor & Navarro (2001). Following Austin et al. (2005), we eliminate the constant C by solving for y, differentiating with respect to x again, and grouping like terms. The resulting constrained Jeans equation is

$$(2\alpha+\gamma-6)\left[\frac{2}{3}(\alpha-\gamma)+1\right](2\alpha-5\gamma) = 15\gamma'' + 3\gamma'(8\alpha-5\gamma-5). \tag{10}$$

In this notation, $\gamma = \gamma(x) = -d\ln y/d\ln x$ and the primes indicate derivatives with respect to $\ln x$.

One way to connect power-law F distributions and equilibria is by making an analogy to fluid systems. In hydrostatic equilibrium, the term on the left-hand side of equation (6) is replaced by a derivative of a single variable, the pressure P (related to the random motion in the system). The important point is that P is related to ρ through an equation of state. This extra relation closes the system of equations and, given boundary conditions, allows one to solve for the equilibrium density distribution. A power-law F distribution acts as a radius-dependent equation of state, linking ρ and the system's random motion, measured by σ.

Austin et al. (2005) demonstrate that this equation has a rich set of solutions that depend on the choices made for α, initial γ [$\gamma(0)$], and initial γ' [$\gamma'(0)$]. In specific density profiles, the

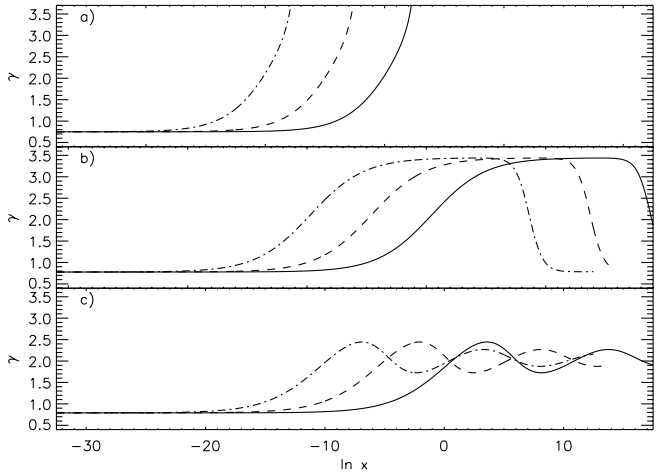

FIG. 7.—Various γ distributions that result from solving eq. (10). Panel *a* shows solutions with $\alpha = 1.875$, panel *b* utilizes $\alpha = 35/18$, and panel *c* has $\alpha = 1.975$. The solid lines in each panel are solutions with $\gamma' = 5 \times 10^{-6}$. The dashed and dash-dotted lines have $\gamma' = 1 \times 10^{-5}$ and $\gamma' = 5 \times 10^{-5}$, respectively. The separations of the various profiles have been exaggerated for clarity.

asymptotic behavior of $\gamma(x)$ can be made to increase without bound, to approach constant values, or even to oscillate. We show several types of solutions in Figure 7. We choose $\gamma(0)$ through the relation $2\alpha - 5\gamma(0) = 0$, representing a zero "pressure" derivative at the center (Austin et al. 2005). Once we choose an α-value, the central γ is set. This figure shows the impact of changing $\gamma'(0)$ from 5×10^{-6} to 5×10^{-5} [see Austin et al. 2005 for examples of solutions with larger $\gamma'(0)$ values]. Smaller values of $\gamma'(0)$ force the $\gamma(x)$ distribution to change less rapidly with increasing x. Since changing $\gamma'(0)$ values simply shifts γ distributions horizontally and does not affect the overall shape [for $\gamma'(0) \lesssim 10^{-3}$], we fix the $\gamma'(0)$ value from here on. Larger $\gamma'(0)$ values can make the γ distribution convex in the region where $r = r_s$, unlike the distributions that are of interest here. Once γ changes from its initial value, the behavior is largely determined by α. As mentioned earlier, γ profiles display one of three kinds of behavior, and we choose to focus on three α-values to provide concrete examples: $\alpha = 1.875$, $\alpha = 35/18$, and $\alpha = 1.975$. $\alpha = 35/18$ divides solutions in which $\gamma(x)$ increases indefinitely (like those in the top panel with $\alpha = 1.875$) from those in which $\gamma(x)$ acts as a damped oscillator (like those in bottom panel with $\alpha = 1.975$). A more extensive discussion of this special α-value can be found in Austin et al. (2005, § 3).

In previous sections, we have discussed many types of density profiles and have just shown that the constrained isotropic Jeans equation has a wide variety of solutions. We are now faced with the following questions: Which (if any) of the density profiles from § 3 provides the best description of the constrained Jeans equation solutions? And does the answer to this question depend on the Jeans equation parameter α?

The thin solid lines in Figure 8 are the γ profiles for the solutions of equation (10) with various α-values and $\gamma'(0) = 1 \times 10^{-5}$. The vertical solid lines denote the radius at which $\gamma = 2$, and the dotted vertical lines mark 0.01 and 10 times this radius. Figure 8*a* has $\alpha = 1.875$. It is clear that the Sérsic form with $n = 2.8$ provides a much better representation of the solution curve than do the Navarro et al. (2004) profiles. In Figure 8*b*, $\alpha = 35/18$ and the quasi-asymptotic behavior of the solution curve looks much more like one would expect for an NFW profile. However, an NFW γ profile has a larger $\gamma'(r_s)$ than the solution curve and does not provide a good approximation. For this case, neither the Sérsic ($n = 4.0$) nor the Navarro et al. (2004) curves are very

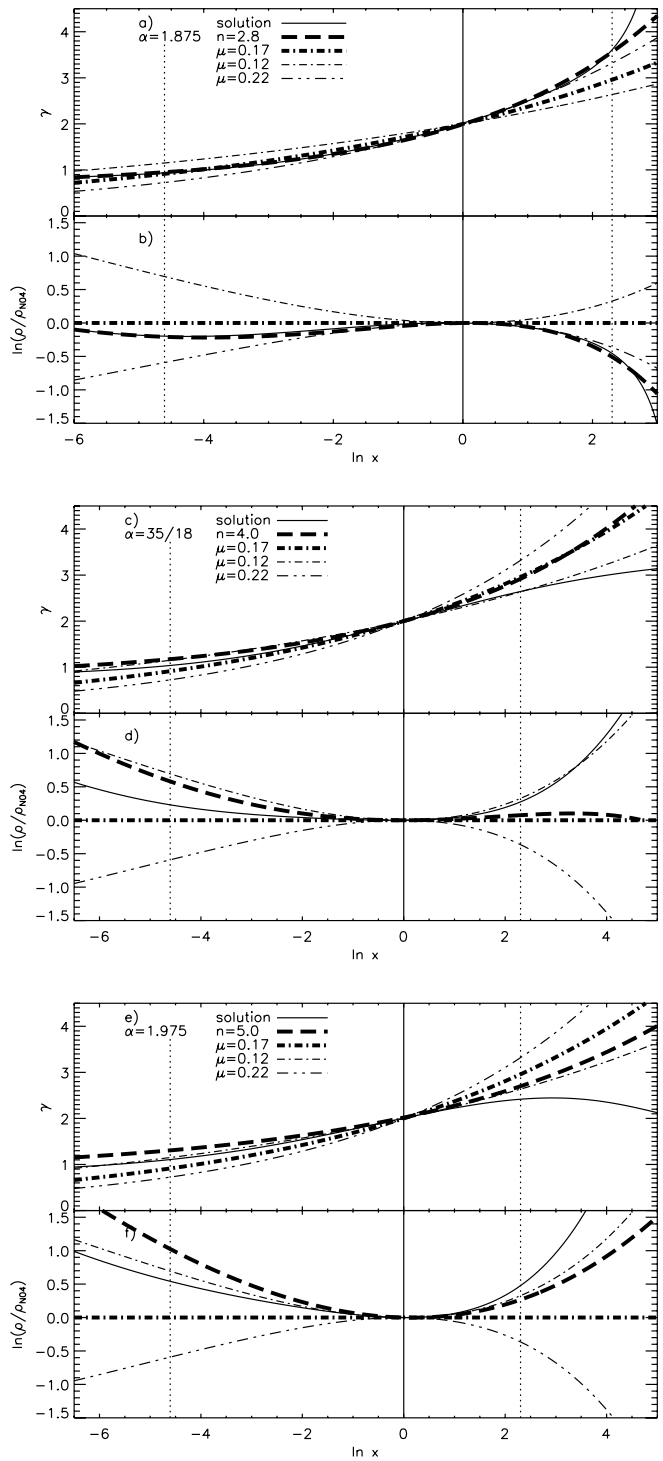

FIG. 8.—Solutions of eq. (10) with $\gamma'(0) = 1 \times 10^{-5}$ (*solid lines*). The top plots in each panel show γ distributions, while the bottom panels present the corresponding density profiles normalized by the N04 distribution. The line types have the same meaning in both plots. The thick-dashed and dash-dotted lines correspond to Sérsic and N04 density distributions, respectively. The thin dash-dotted lines are Navarro et al. (2004) profiles with $\mu = 0.12$; the thin double-dot–dashed lines have $\mu = 0.22$. Note that the range of $\ln x$ is much smaller than in Fig. 7; the vertical solid lines mark the positions of r_s or r_2; the dotted vertical lines are 1/100 and 10 times this radius. In panels *a* and *b*, $\alpha = 1.875$ and the Sérsic $n = 2.8$. Panels *b* and *c* have ($\alpha = 35/18$, $n = 4.0$), and panels *e* and *f* have ($\alpha = 1.975$, $n = 5.0$).

good matches to the solution. The bottom panel shows the solution for $\alpha = 1.975$. Again, the behavior of the solution curve is poorly represented by either the Sérsic ($n = 5.0$) or Navarro et al. (2004) curves. The Sérsic behavior is not very surprising since Figure 4 shows that no Sérsic profile can produce α-values as large as 1.975. While these last two plots point out the inadequacies of our fitting functions for general solutions of the constrained Jeans equation, in the case with $\alpha = 1.875$, an average value from N-body simulations, the Sérsic profile provides a substantially better fit over the N04 profile to the solution of the isotropic constrained Jeans equation.

5. SUMMARY AND CONCLUSIONS

The apparent commonness of power-law distributions in the phase-space density proxy $F \equiv \rho/\sigma^3 \propto r^{-\alpha}$ (density divided by velocity dispersion cubed) in collapsed collisionless systems (e.g., Taylor & Navarro 2001; Austin et al. 2005) has led us to investigate (1) whether or not arbitrary equilibrium density profiles automatically lead to such behavior and (2) the types of equilibria that occur under the constraint that F is scale-free. In this study we have only investigated isotropic, spherically symmetric systems, but we will soon extend this work to include anisotropic distributions.

We find that the F distribution corresponding to the Hernquist (or King) profile is not an acceptable power law and refutes the idea that mechanical equilibrium alone is responsible for power-law F distributions. In general, profile types that empirically provide good fits to N-body halos produce power-law F behavior, with the Navarro et al. (2004) and Sérsic types being superior to the generalized dual–power-law profiles in this regard. We speculate that this ubiquity is not coincidence but rather that scale-free F is a generic result of the physics of collisionless collapse. For the isotropic systems considered here, the Sérsic profile F distributions with the smallest $\Delta_{\rm rms}$ values tend to have smaller α-values than those corresponding to Navarro et al. (2004) profiles. However, each type of density profile covers the range of α-values found in N-body simulations.

Taking power-law F behavior as a given allows us to write a constrained Jeans equation that only involves the logarithmic density slope γ, its derivatives, and α. This approach of deriving equilibrium density (actually, γ) distributions and comparing them to the γ profiles corresponding to the Navarro et al. (2004) and Sérsic density profiles complements our earlier findings. The $\alpha = 1.875$ results (Fig. 8, *top panel*) echo our previous conclusions that N-body halos formed in cosmological simulations are best described by Sérsic models.

The preceding points depend on ρ/σ^3 versus r being the relevant relationship. As we do not have a compelling explanation for this relation, we have also investigated other correlations of F with possibly more physical quantities. These quantities have so far failed to best the power-law correlation between F and r. Another possibility is that F itself is not the most illuminating variable. Based on a thoughtful suggestion from R. Henriksen, we have also looked at whether or not the exponent of σ in the combination ρ/σ^m can be changed to produce a better power law. Our results clearly point to $m = 3$ as the most interesting value.

One other question to ask is whether or not any type of relaxation to equilibrium results in scale-free ρ/σ^3. In particular we have wondered what effect two-body relaxation may have. This is not to suggest that current N-body simulations are affected by two-body relaxation, but see El-Zant (2005). One argument against the importance of two-body relaxation in forming power-law F is demonstrated by King profiles, which accurately model two-body relaxed globular clusters, but do not produce $F \propto r^{-\alpha}$. This is reminiscent of the findings of Binney (1982). That study found significant differences between the de Vaucouleurs and King models' $N(E)$ distributions [$N(E)\,dE$ is the number of particles with energies near E]. Combining these findings with our own results for the King profile, as well as the results of Austin et al. (2005; halo formation without any two-body effects produces scale-free F), brings us to conclude that relaxation effects other than two-body interactions are responsible for the power-law F distributions.

We have demonstrated that, in equilibrium, density profiles that accurately describe the end results of simulated collisionless collapses (and hence violent relaxation) produce power-law F distributions, while those that have been designed mostly for analytical tractability (e.g., Hernquist profiles) or to describe systems significantly different than galaxies (e.g., King models) do not. And although there is no general theory explaining power-law F behavior, our findings encourage us to speculate that dynamical collapse processes (violent relaxation in particular) are playing a major role in making ρ/σ^3 of equilibrium systems scale-free.

This work has been supported by NSF grant AST 03-07604. Research support for A. B. comes from the Natural Sciences and Engineering Research Council (Canada) through the Discovery grant program. A. B. would also like to acknowledge support from the Leverhulme Trust (UK) in the form of the Leverhulme Visiting Professorship at the Universities of Oxford and Durham. J. J. D. was partially supported through the Alfred P. Sloan Foundation. We would like to thank Alister Graham and an anonymous referee for several helpful comments. Extra thanks to Dick Henriksen for motivating us to investigate variations in F.

REFERENCES

Ascasibar, Y., Yepes, G., Gottlöber, S., & Müller, V. 2004, MNRAS, 352, 1109
Austin, C. G., Williams, L. L. R., Barnes, E. I., Babul, A., & Dalcanton, J. J. 2005, ApJ, 634, 756
Barnes, E. I., Williams, L. L. R., Babul, A., & Dalcanton, J. J. 2005, ApJ, 634, 775
Bertschinger, E. 1985, ApJS, 58, 39
Binney, J. 1982, MNRAS, 200, 951
Binney, J., & Tremaine, S. 1987, Galactic Dynamics (Princeton: Princeton Univ. Press)
Dalcanton, J. J., & Hogan, C. J. 2001, ApJ, 561, 35
Dehnen, W., & McLaughlin, D. E. 2005, MNRAS, 363, 1057
Diemand, J., Moore, B., & Stadel, J. 2004a, MNRAS, 352, 535
———. 2004b, MNRAS, 353, 624
El-Zant, A. A. 2005, preprint (astro-ph/0506617)
Graham, A. W., Merritt, D., Moore, B., Diemand, J., & Terzić, B. 2005, AJ, submitted (astro-ph/0509417)
Hansen, S. H., & Moore, B. 2006, NewA, 11, 333
Hernquist, L. 1990, ApJ, 356, 359
Hoeft, M., Mücket, J. P., & Gottlöber, S. 2004, ApJ, 602, 162
Jeans, J. H. 1919, Phil. Trans. R. Soc. London A, 218, 157
King, I. R. 1966, AJ, 71, 64
Lynden-Bell, D. 1967, MNRAS, 136, 101
Merritt, D., Navarro, J. F., Ludlow, A., & Jenkins, A. 2005, ApJ, 624, L85
Moore, B., Governato, F., Quinn, T., Stadel, J., & Lake, G. 1998, ApJ, 499, L5 (M98)
Navarro, J. F., Frenk, C. S., & White, S. D. M. 1996, ApJ, 462, 563
———. 1997, ApJ, 490, 493
Navarro, J. F., et al. 2004, MNRAS, 349, 1039 (N04)
Raisa, E., Tormen, G., & Moscardini, L. 2004, MNRAS, 351, 237
Sérsic, J. L. 1968, Atlas de Galaxies Australes (Córdoba: Obs. Astron., Univ. Nac. Córdoba)
Taylor, J. E., & Navarro, J. F. 2001, ApJ, 563, 483
Trujillo, I., Asensio Ramos, A., Rubiño-Martín, J., Graham, A., Aguerri, J., Cepa, J., & Gutiérrez, C. 2002, MNRAS, 333, 510